9-28-2018

Dual Gain and Loss of Cullin 3 Function Mediates Familial Hyperkalemic Hypertension

Ryan J. Cornelius
Oregon Health and Science University

Chang Zhang
Shanghai Jiao Tong University School of Medicine

Kayla J. Erspamer
Oregon Health and Science University

Larry N. Agbor
Carver College of Medicine, University of Iowa

Curt D. Sigmund
Carver College of Medicine, University of Iowa

See next page for additional authors

Dual gain and loss of cullin 3 function mediates familial hyperkalemic hypertension

Ryan J. Cornelius[1], Chong Zhang[2], Kayla J. Erspamer[1], Larry N. Agbor[3], Curt D. Sigmund[3], Jeffrey D. Singer[4], Chao-Ling Yang[1,*], and David H. Ellison[1,5,*]

1. Division of Nephrology and Hypertension, Department of Medicine, Oregon Health and Science University, Portland, OR, USA
2. Department of Nephrology, Xin Hua Hospital Affiliated to Shanghai Jiao Tong University School of Medicine, Shanghai, China
3. Department of Pharmacology, UIHC for Hypertension Research, Carver College of Medicine, University of Iowa, Iowa City, IA, USA
4. Department of Biology, Portland State University, Portland, OR, USA
5. VA Portland Health Care System, Portland, OR, USA

*Chao-Ling Yang and David H. Ellison contributed equally to this work.

Running Foot: Cul3Δ403-459 degrades KLHL3 via dual pathways

David H. Ellison, M.D.
Division of Nephrology and Hypertension, SON440
Oregon Health and Science University
3181 SW Sam Jackson Park Road
Portland, OR 97239
Phone: 503 494-4465
Email: ellisond@ohsu.edu

Abbreviations:

Cul3, Cullin 3; FHHt, familial hyperkalemic hypertension; CSN, COP9 signalosome; WNK, with-no-lysine kinase; NCC, Na-Cl cotransporter; DCT, distal convoluted tubule; SPAK, serine/threonine protein kinase 39; OSR1, oxidative stress-response 1; CRL, cullin-RING ligase; KLHL3, kelch-like 3; NEDD8, neuronal precursor cell expressed developmentally down-regulated protein 8; JAB1, jun activation domain-binding protein-1; 4HB, 4-helix bundle; WT, wild type; BTB, bric-a-brac, tramtrack, broad-complex; CAND1, cullin-associated and NEDD8-dissociated protein 1; Keap1, kelch-like ECH-associated protein-1; Nrf2, nuclear factor erythroid 2-related factor 2; 3-MA, 3-methyladenine.

Abstract

Familial hyperkalemic hypertension is caused by mutations in WNK kinases, or in proteins that mediate their degradation, KLHL3 and cullin 3 (Cul3). While the mechanisms by which WNK and KLHL3 mutations cause the disease are now clear, the effects of the disease-causing Cul3Δ403-459 mutation remain controversial. Possible mechanisms including hyperneddylation, altered ubiquitin ligase activity, decreased association with the COP9 signalosome (CSN), and increased association with and degradation of KLHL3 have all been postulated. Here, we systematically evaluated the effects of Cul3Δ403-459 using cultured kidney cells. We first identified that the catalytically active CSN subunit JAB1 does not associate with the deleted Cul3 4HB domain, but instead with the adjacent α/β_1 domain, suggesting that altered protein folding underlie the impaired binding. Inhibition of deneddylation, with JAB1 siRNA, increased Cul3 neddylation, and decreased KLHL3 abundance, similar to the Cul3 mutant. We next determined that KLHL3 degradation has both ubiquitin ligase-dependent and -independent components. Proteasomal KLHL3 degradation was enhanced by Cul3Δ403-459; however, autophagic degradation was also upregulated by this Cul3 mutant. Finally, to evaluate whether deficient substrate adaptor was responsible for the disease, we restored KLHL3 to WT-Cul3 levels. In the absence of WT-Cul3, WNK4 was not degraded, demonstrating that Cul3Δ403-459 itself cannot degrade WNK4; conversely, when WT-Cul3 was present, as in diseased humans, WNK4 degradation was restored. In conclusion, deletion of exon 9 from Cul3 generates a protein that is itself ubiquitin ligase-defective, but also capable of enhanced autophagocytic KLHL3 degradation, thereby exerting dominant-negative effects on the WT-allele.

Keywords: Cullin-RING ubiquitin ligase, Neddylation, Deneddylation, JAB1

Introduction

With-no-lysine (WNK) kinases control blood pressure and potassium homeostasis, predominantly by regulating membrane expression and activity of the thiazide-sensitive Na-Cl cotransporter (NCC) in the distal convoluted tubule (DCT). These kinases signal via serine/threonine protein kinase 39 (SPAK; *STK39*) and oxidative stress-response 1 (OxSR1 or OSR1; *OXSR1*), which directly phosphorylate and activate the transport protein (19, 30). The human Mendelian disease Familial Hyperkalemic Hypertension (FHHt, also called pseudohypoaldosteronism type 2 or Gordon syndrome) results from activation of this signaling pathway in the distal nephron (21). FHHt patients exhibit hyperkalemia, metabolic acidosis, and hypertension, symptoms that largely disappear during treatment with thiazide diuretics (13). FHHt can be caused by mutations in WNK1 or WNK4 (32), or in the cullin-RING ligase (CRL) proteins cullin 3 (*Cul3*) (4) and kelch-like 3 (*KLHL3*) (28). Cul3 is part of an E3 ubiquitin ligase complex that regulates protein degradation. CRLs do not degrade proteins directly, but instead attach strings of ubiquitin moieties to a protein, thereby targeting it for degradation, typically within the proteasome. Cullin acts as a scaffold protein for the other CRL subunits. It is now clear that WNK kinases are targets for CRLs. The substrate adaptor KLHL3, binds both WNK kinases and Cul3, bringing the WNK into proximity to the catalytic region of the CRL, thereby permitting ubiquitylation (18, 25). The WNK4 or KLHL3 mutations that cause disease, do so by disrupting these binding reactions, permitting WNKs to accumulate (31). The Cul3 mutations that cause FHHt, however, do not decrease substrate adaptor binding (27, 31); although mouse models indicate that WNKs are not degraded normally (24), the precise mechanisms involved remain controversial.

An important feature of CRL activity is the attachment of NEDD8 (neuronal precursor cell expressed developmentally down-regulated protein 8) through a process called neddylation. NEDD8 attachment is required to activate CRLs by increasing the flexibility of the cullin-ring structure, allowing the transfer of ubiquitin from the RING protein to the target substrate (3, 20, 23). The reverse process, deneddylation, is facilitated by the multi-subunit COP9 signalosome (CSN) complex. The CSN interacts with CRLs and removes NEDD8 through its catalytically-active CSN5 subunit, also known as JAB1 (jun activation domain-binding protein-1) (6). Although a simple model originally suggested that neddylated Cul3 is active, whereas unneddylated Cul3 is inactive, inhibition of CSN paradoxically increases, rather than decreases, the abundance of substrate proteins *in vivo* (22). It appears instead that, while neddylation of cullins is indeed essential to activate them, it also makes them unstable and prone to degradation (35). Thus, the effects of neddylation on cullin activity and abundance are complex.

All known FHHt-causing Cul3 mutations cause deletion of exon 9, resulting in a mutant protein that lacks 57 amino acid residues (Cul3Δ403-459) (4). Previous work by our group (14), and confirmed by others (24), showed that Cul3Δ403-459, expressed in cells, is hyperneddylated, compared with wild type (WT), suggesting either that it is more susceptible to neddylation or that it is resistant to deneddylation. Schumacher *et al.* (24) confirmed that Cul3Δ403-459 had impaired deneddylation and compromised CSN binding, suggesting

that the deleted segment was responsible. Exon 9 of Cul3 encodes the 4-helix bundle (4HB) domain. Min et al. (15) demonstrated that the CSN binding site for the closely related cullin 1 protein was located within the 4HB and α/β_1 domains. However, the CSN binding site for Cul3 has yet to be determined.

Cul3Δ403-459 has an increased association with bric-a-brac, tramtrack, broad-complex (BTB)-Kelch substrate adaptor proteins, including KLHL3 (10, 14, 24). The FHHt Cul3 mutant strongly ubiquitylated KLHL3 (14, 24) leading to decreased abundance, *in vitro* (14). However, administration of the non-specific neddylation inhibitor, MLN4924, which prevents NEDD8 conjugation and presumably inactivates CRLs, only partially normalized KLHL3 abundance. Additionally, the enhanced interaction of KLHL3 with Cul3Δ403-459 remained in the absence of neddylation. The results indicate that Cul3Δ403-459 may have neddylation-dependent and neddylation-independent effects. Here, we examined the mechanisms and consequences of Cul3Δ403-459 hyperneddylation, and identified novel ligase dependent, and ligase independent mechanisms for the human disease.

Materials and Methods

Antibodies

Antibodies used are described in Table 1.

Cell culture, plasmids, and transfections

For cell culture experiments HEK293 cells were used unless otherwise stated. CRISPR-Cas9-edited Cul3 knockdown HEK293T cells ($HEK293T^{Cul3\text{-}KO}$) were previously reported (10). Cells were maintained in DMEM supplemented with 10% FBS, 25 mM HEPES, 100 units/ml penicillin, 100 µg/ml streptomycin. Cells were transiently transfected using Lipofectamine 2000 (Ambion, Foster City, CA, USA; Invitrogen). Cul3 constructs were made by amplifying FLAG-Cul3 WT DNA using Phusion Hot Start II DNA Polymerase (Thermo Fisher Scientific, Boston, MA, USA) with the appropriate primers, purified with the PureLink PCR Purification Kit (Invitrogen) and properly digested. The products were then extracted using the UltraClean GelSpin DNA Extraction Kit (MoBio Laboratories, Inc., Carlsbad, CA, USA) and ligated into N-terminal GST tag mammalian plasmid, pSF-CMV-Puro-NH2-GST (Oxford Genetics, Oxford, UK), with T4 DNA Ligase (New England BioLabs, Ipswich, MA, USA). Ligated constructs were transformed using DH5α competent cells (Thermo Fisher Scientific) and plasmid DNA was purified with either the QIAprep Spin Miniprep Kit or HiSpeed Plasmid Midi Kit (Qiagen, Hilden, Germany). Sanger sequencing was performed for all constructs.

For siRNA experiments, either 40 nM of COPS5 siRNA (Ambion) or control siRNA was transfected along with DNA plasmids. Cells were harvested at 36 h post-transfection.

For cycloheximide chase experiments, cycloheximide was added 36 h after transfection at a concentration of 100 µg/ml and the cells were lysed at the time points indicated.

For MG132, chloroquine, 3-methyadenine, MLN4924, and tBHQ experiments, drug was added to cells 18 h before harvesting at the concentrations given.

For ubiquitin assay experiments, cells were co-transfected with HA-tagged ubiquitin DNA plasmid. Cells were lysed 48 h after transfection in cell lysis buffer containing 10 mM N-ethylmaleimide. Immunoprecipitation and Western blotting was carried out as below.

Immunoprecipitation and Western blotting

Transfected cells were harvested in 0.5% Triton X-100 in PBS cell lysis buffer containing enzyme inhibitors. For immunoprecipitation cell lysate was pre-cleared with protein A-sepharose beads for 1-2 hours. Cell lysate was then incubated with Glutathione Sepharose 4B medium (GE Healthcare, Piscataway, NJ, USA) for 2 h at room temperature, primary antibody and Protein A-Sepharose 4B medium (GE Healthcare) or anti-FLAG Affinity Gel (Biotool, Houston, TX, USA) overnight at 4° C. Protein samples were separated by electrophoresis on 4-12% NuPAGE bis-tris polyacrylamide gels (Thermo Fisher Scientific) or 4-15% Criterion TGX stain-free gels (Bio-Rad Laboratories, Hercules, California, USA) and transferred to Immobilon-P PVDF membranes (EMD Millipore, Billerica, MA, USA). For all experimental conditions performed in triplicate, each well represents a unique transfection. Stain-free imaging was used as a total protein loading control, unless otherwise stated. Membranes were blocked with 5% milk in PBS for 1 h at room temperature before incubation with primary antibody in blocking buffer for 1 h at room temperature or overnight at 4° C. Appropriate HRP-conjugated secondary antibody in blocking buffer was added to membranes for 1 h at room temperature. Membranes were developed using enhanced chemiluminescence, Western Lightning Plus–ECL (Perkin Elmer, Waltham, MA, USA), and proteins were visualized using PXi digital imaging system (Syngene, Frederick, MA, USA).

Statistics

Data are presented as individual values as well as mean ± SEM. Differences between two groups were determined using two-tailed unpaired Student's t-test and differences between multiple groups were analyzed using one-way ANOVA followed by Tukey's multiple comparisons test. A *P* value of less than 0.05 was considered significant. Statistical analysis was performed using GraphPad Prism 7 software (GraphPad Software, San Diego, CA, USA).

Results

CSN binds to Cul3 at the α/β_1 domain.

CRLs are activated by NEDD8 attachment, but for full functionality, they must also be deneddylated. The deneddylation of Cul3 appears to be disrupted in Cul3Δ403-459 FHHt, as the mutant protein is more highly neddylated than WT, at least when expressed in cultured cells (14, 24). Schumacher et al. reported that

Cul3Δ403-459 exhibits decreased interaction with JAB1 (24), suggesting that the deleted domain may include the CSN binding site. The crystal structure of CSN with the highly homologous cullin 1 (12) and cullin 4A (5), showed that the CSN2 subunit interacts directly with the C-terminal domain. Additionally, Min et al. (15) determined that the CSN binding site for cullin 1 (which is structurally similar to Cul3) was located specifically within the C-terminal domains 4HB and α/β_1. Inspection of the Cul3 gene revealed that exon 9 (deleted in FHHt-causing Cul3 mutations) encodes the 4HB domain (see Figure 1A). To determine sites of CSN interaction with Cul3, we generated Cul3 deletion constructs (Figure 1A). We first confirmed that, compared with WT-Cul3, there was minimal JAB1 precipitation by Cul3Δ403-459 (Figure 1B). Similarly, the Cul3 construct containing N-terminal residues 1-402, which lacks the 4HB domain and the adjacent α/β_1 domain showed nominal precipitation of JAB1 (Figure 1C). Surprisingly, inclusion of the 4HB domain with the N-terminal region also showed low binding to JAB1 (Figure 1C, Cul3 1-459). These results indicate clearly that Cul3 amino acids 403-459 (containing the 4HB domain) are not sufficient for binding to the CSN. This suggests that the Cul3Δ403-459 mutation does not impair Cul3-CSN binding directly, but rather disrupts protein folding within a site C-terminal to the 4HB domain; this suggestion is consistent with structural modeling of wild type and mutant Cul3 (24).

To identify the specific binding site for the CSN and confirm that the 4HB does not bind JAB1 we developed individual Cul3 domain constructs for 4HB and α/β_1. Additionally, we generated a construct containing both the 4HB and α/β_1 domains (4HB:α/β_1), an N-terminal construct containing cullin repeat sequences (R1:R2:R3) and a C-terminal construct containing domains WH-A, α/β_2, and WH-B (WH-A:α/β_2:WH-B). JAB1 immunoprecipitated with the Cul3 construct containing both the 4HB and α/β_1 domains and with α/β_1 alone, but not with 4HB alone (Figure 1D). JAB1 was not precipitated with Cul3 constructs that lacked the α/β_1 domain, R1:R2:R3 and WH-A:α/β_2:WH-B. The results indicate that the first α/β domain of Cul3 is the binding site for JAB1 and therefore the CSN.

To verify that the α/β_1 domain is the binding site for the CSN we developed a full-length Cul3 construct in which the α/β_1 was deleted (Cul3Δ461-586). JAB1 was not precipitated with Cul3Δ461-586 (Figure 1E). As expected, Cul3Δ461-586 also showed enhanced neddylation compared to WT-Cul3. These results further confirm that the CSN binding site is contained within the α/β_1 domain of Cul3.

CSN inhibition enhances Cul3 neddylation and reduces KLHL3 and WNK4 abundance.

Neddylation of cullins has paradoxical effects, with both neddylation and deneddylation being required for normal CRL function. Because Cul3Δ403-459 exhibits decreased interaction with JAB1 (24), we examined the effects of inhibiting JAB1 activity on Cul3 in HEK293 cells. Cells were transfected with siRNA to reduce endogenous JAB1. Western blotting for endogenous Cul3 exhibited a more neddylated Cul3 (as detected by an increase in the higher molecular weight Cul3 band) when JAB1 was reduced, compared to control (Figure 2). Similarly, probing the blot with an antibody against NEDD8 showed a greater abundance of neddylated Cul3

when JAB1 was knocked down, as the antibody recognized a product at the molecular weight of Cul3. The effects of JAB1 inhibition on the protein abundance of the Cul3 substrate adaptor KLHL3 and substrate WNK4 were also determined. Abundance of overexpressed KLHL3 and WNK4 were lower, in cells transfected with JAB1 siRNA, compared to control siRNA, indicating that JAB1 knockdown and increased neddylation activates Cul3 in transfected cells.

Cul3Δ403-459 causes decreased stability of KLHL3

We showed previously that KLHL3 protein abundance was lower when co-expressed with Cul3Δ403-459 than with WT Cul3 in HEK293 cells (14), suggesting that degradation was more rapid in the presence of mutant Cul3. To test this, we measured the stability of KLHL3 using the cycloheximide chase assay. KLHL3 abundance was significantly lower 24 hours after cycloheximide treatment when co-transfected with Cul3Δ403-459 compared to WT Cul3, but the apparent degradation rates at other time points were not different (Figure 3A). As KLHL3 co-transfected with WT Cul3 was stable at least 24 h after cycloheximide treatment (the long stability of KLHL3 has been previously published (17)), which can lead to anomalous results in cycloheximide chase experiments (37), we decided to examine a canonical CRL substrate, WNK4, using a similar approach. Similar to the Cul3-KLHL3 experiments, WNK4 was stable when cycloheximide was introduced in the absence of KLHL3; however, when co-transfected together with KLHL3, WNK4 abundance was strikingly reduced (Figure 3B). When we compared the effects of KLHL3 on WNK4 abundance with those of Cul3Δ403-459 on KLHL3 abundance, the results are remarkably similar (Figure 3C). In fact, when other groups have examined the effects of KLHL3 on WNK4 abundance, they also noted remarkably reduced WNK4 abundance in the presence of KLHL3 (31). Thus, although we cannot prove that the Cul3Δ403-459 and WT Cul3 have differential effects on KLHL3 synthesis, the current results, when coupled with those shown below suggest that KLHL3 is degraded more rapidly by the Cul3 mutant.

Ligase-dependent and -independent effects of Cul3Δ403-459 on KLHL3 and WNK4.

The Cul3Δ403-459 mutation has altered ubiquitin ligase activity as shown by increased ubiquitylation of KLHL3 and decreased ubiquitylation of WNK4 (14, 24). Yet, Cul3Δ403-459 also has ligase-independent effects, such as enhanced binding to BTB-Kelch adaptors and decreased binding to CSN subunits and cullin-associated and NEDD8-dissociated protein 1 (CAND1) (10, 14, 24). To try to better understand the anomalous effects of the Cul3Δ403-459 protein we generated a neddylation-deficient Cul3Δ403-459 double mutant, Cul3Δ403-459 K712R. Neddylation is generally considered to be necessary to activate CRLs. The RING subunit utilizes specific E1 and E2 enzymes to covalently attach a NEDD8 protein to lysine 712 of Cul3 (33). Cul3Δ403-459 K712R includes a point mutation at the neddylation-site preventing NEDD8 attachment, and rendering the construct ligase-deficient. Immunoprecipitation of FLAG-tagged Cul3Δ403-459 K712R showed an almost complete loss of neddylation (Figure 4A), indicating that the vast majority of Cul3Δ403-459

neddylation occurs at the lysine 712 residue. Co-immunoprecipitation of the different Cul3 constructs and KLHL3 showed that similar to Cul3Δ403-459, Cul3Δ403-459 K712R bound to more KLHL3 protein compared to WT-Cul3 (Figure 4B), confirming that neddylation, and therefore ubiquitin ligase activity, is not required for increased protein binding.

Ubiquitylation of the BTB-adaptor KLHL3 (Figure 4C) was greater in cells transfected with Cul3Δ403-459, compared to WT-Cul3, as reported previously (14). As expected, this greater KLHL3 ubiquitylation was not apparent when the neddylation deficient Cul3Δ403-459 K712R was transfected. Yet the current results also suggest that ubiquitin ligase activity is not fully responsible for the anomalous Cul3Δ403-459 activity. In cells transfected with both KLHL3 and WNK4, the abundance of KLHL3 was lower, when Cul3Δ403-459 was present than with WT-Cul3, consistent with increased substrate adaptor ubiquitylation and degradation by the mutant protein (Figure 4D). Cul3Δ403-459 also led to more WNK4 abundance than did WT-Cul3 (Figure 4D), as we, and others, have reported previously. When the ligase-deficient Cul3Δ403-459 K712R construct was transfected, however, the effects on KLHL3 and WNK4 were reduced compared to Cul3Δ403-459 toward normal (WT-Cul3) levels, (Figure 4D). Unexpectedly, the effects of Cul3Δ403-459 on KLHL3 were not completely removed by the ligase-deficient Cul3Δ403-459 K712R double mutant, indicating that the effects of Cul3Δ403-459 is only partially dependent on ubiquitin ligase activity.

Cul3Δ403-459-mediated KLHL3 degradation is both proteasome- and autophagy-dependent.

As shown above, when ubiquitin ligase activity is lacking, as in the Cul3Δ403-459 K712R double mutant, there is less abundance of KLHL3, however, the amount of KLHL3 abundance retained by the construct (ligase-independent degradation) is still significant. Since the neddylation-deficient construct should block the ubiquitin-proteasome degradation pathway, the remaining Cul3Δ403-459-mediated KLHL3 degradation could be autophagy-dependent. The proteasome is the canonical pathway for degrading ubiquitylated proteins, and it has been shown to contribute to WNK kinase degradation (14); yet there is also evidence that KLHL3 and WNK4 can be degraded via autophagy (16). To determine the pathways involved in Cul3Δ403-459-mediated KLHL3 degradation, we used the inhibitors MG132 and chloroquine. Proteasomal inhibition with 10 μM MG132 had no effect on the control group, but partially suppressed Cul3Δ403-459-mediated KLHL3 degradation (Figure 5). Inhibition of autophagy with 100 μM chloroquine, however, had a small but significant effect on the control group, indicating that KLHL3 is constitutively degraded via autophagy (Figure 6A). Incubation of Cul3Δ403-459 with chloroquine also resulted in a partial suppression of KLHL3 degradation. The percent change in KLHL3 protein abundance due to chloroquine administration was significantly different between control and Cul3Δ403-459 (Figure 6B), which indicates an increased autophagic degradation of KLHL3 mediated by the Cul3 mutant. To confirm these results, we treated cells with another autophagy blocker, 3-methylandenine (3-MA), an inhibitor of autophagosome formation (Figure 6C). The results closely resembled chloroquine administration further indicating autophagic KLHL3 degradation.

Treatment of the cells with both MG132 and chloroquine completely abolished Cul3Δ403-459-mediated KLHL3 degradation (Figure 6D). The data suggest that, under the conditions provided, KLHL3 is degraded by Cul3Δ403-459 through both the ubiquitin-proteasome pathway and the autophagy pathway. Thus, WT-Cul3 and Cul3Δ403-459 degrade WNK4 and KLHL3, respectively, via two different pathways. WNK4 is ubiquitylated and degraded through the proteasomal pathway. KLHL3 is degraded by both the proteasome and the autophagy pathway.

Increasing KLHL3 expression normalizes Cul3Δ403-459-mediated inhibition of WNK4 degradation in the presence of WT-Cul3.

We suggested previously that the increased activity of Cul3Δ403-459 toward KLHL3 reduced the availability of KLHL3 to participate in degrading WNK kinases (14). Alternatively, others have suggested that the increased association of Cul3Δ403-459 with KLHL3 may sequester it, and accomplish the same effect. If the low level of KLHL3 contributes to the increase in WNK4 in Cul3Δ403-459 patients, then increasing the amount of KLHL3 should reduce WNK4. By increasing the amount KLHL3 DNA transfected into the cells we were able to increase KLHL3 protein abundance. In HEK293 cells that lack Cul3 (HEK293T$^{Cul3\text{-}KO}$), an increase in KLHL3 protein levels caused only a slight reduction in WNK4 abundance (28%); WNK4 was still substantially higher than in cells transfected with WT-Cul3, even though KLHL3 protein abundance was similar (compare the first and last three lanes in Figure 7A). However, in HEK293 cells that contained endogenous WT-Cul3 (Figure 7B), increasing KLHL3 protein levels in cells transfected with Cul3Δ403-459 caused a striking reduction in WNK4 protein abundance (64%), to a value that was not significantly different from WT-Cul3 transfected cells. The data show that Cul3Δ403-459 itself is unable to substantially degrade WNK4, even when KLHL3 is normalized, but when Cul3Δ403-459 and Cul3 are both present in cells, as they are in heterozygous humans, the addition of KLHL3 normalizes degradation of WNK4. This suggests that, *in vitro*, Cul3Δ403-459 degrades KLHL3, preventing WT-Cul3 from binding to WNK4.

Cul3Δ403-459 exhibits a dominant effect in cells.

It has been suggested that Cul3Δ403-459 causes FHHt by inducing functional Cul3 haploinsufficiency, (10, 24). This suggestion derives from the observation that the abundance of Cul3Δ403-459 is very low in a knock-in mouse model of FHHt, and also that introducing a 1:1 molar ratio of WT-Cul3 to Cul3Δ403-459 did not inhibit ubiquitylation of WNK4 (24). Yet Uchida and colleagues noted that mice with functional Cul3 haploinsufficiency do not exhibit signs of FHHt (2), and as noted above, Cul3Δ403-459 may either degrade and/or sequester KLHL3, thereby exerting a dominant negative effect (10, 14). To determine whether Cul3Δ403-459 has dominant effects in cells, we transfected both WT-Cul3 and Cul3Δ403-459 together at different ratios. In the presence of constant WT-Cul3, increasing Cul3Δ403-459 reduced KLHL3 abundance and increased WNK4 abundance (Figure 8), and increasing WT-Cul3 in the presence of Cul3Δ403-459

increased KLHL3 and decreased WNK4. Thus, Cul3Δ403-459 clearly exerts a dominant effect in cultured cells; this is consistent with the autosomal dominant inheritance of FHHt type 4.

Cul3Δ403-459 does not affect Keap1 and cyclin E protein abundance

Because Cul3 can interact with and ubiquitinate multiple substrates through many different substrate adaptors, then it would be expected that the Cul3Δ403-459 mutant would affect other proteins besides KLHL3 and WNK4. To better understand the effects of the Cul3Δ403-459 mutant, we examined three other proteins that interact with Cul3. The oxidative stress response protein, nuclear factor erythroid 2-related factor 2 (Nrf2), is another substrate of Cul3 and interacts through the BTB-Kelch substrate adaptor protein kelch-like ECH-associated protein-1 (Keap1). Unlike KLHL3, Keap1 showed no change in protein abundance when cells were transfected with Cul3Δ403-459 or Cul3Δ403-459 K712R (Figure 9). Although Keap1 was unchanged, its substrate Nrf2 showed an increase in protein abundance in Cul3Δ403-459 transfected cells. The amplified Nrf2 was also observed in cells transfected with Cul3Δ403-459 K712R. Cyclin E, which is a canonical Cul3 substrate and is involved in cell cycle regulation, was unchanged when transfected with Cul3Δ403-459 or Cul3Δ403-459 K712R. The results demonstrate that the Cul3Δ403-459 mutant has differential effects on its substrates and substrate adaptors.

Discussion

Mutations in *WNK1, WNK4, Cul3*, and *KLHL3* cause FHHt, predominantly by increasing NCC activity along the DCT, suggesting that these proteins comprise a single signaling pathway. The disease pathogenesis, in all cases, appears to result from an increase in WNK kinase abundance, either owing to enhanced transcription, or impaired degradation. While *WNK4* and *KLHL3* mutations impair the degradative arm of this pathway by disrupting the ability of WNK kinases to form complexes with KLHL3 and Cul3, the mechanisms involved in *Cul3* disease have been more difficult to unravel (17, 18, 25, 28, 29, 31, 34). We reported previously that the FHHt-mutant Cul3 ubiquitylates and facilitates KLHL3 degradation more actively than does WT-Cul3, and suggested that the mutant exhibits dominant effects (14). The dominant nature of the Cul3Δ403-459 mutation was very recently confirmed, using mouse models (9). Here we determined that Cul3Δ403-459 has an altered structure that decreases interaction with the CSN. Yet the results also discern a novel, secondary, ligase-independent autophagocytic KLHL3 degradation pathway that appears essential for the autosomal dominant phenotype.

The current results confirm our prior work (14), indicating that that Cul3Δ403-459 is hyperneddylated, when expressed in cells. Ibeawuchi and colleagues (10), in contrast, could not detect hyperneddylation of Cul3Δ403-459 and suggested that the mutant protein is neddylated less efficiently than WT. A potential resolution to this paradox is apparent from the work of Schumacher and colleagues (24), who also documented that Cul3Δ403-459 is hyperneddylated in cells, but found that the neddylation process itself was less efficient.

They demonstrated that the defect lies in a failure of the CSN to associate with Cul3, and therefore, a failure of deneddylation. The current work confirms that Cul3Δ403-459 does not associate normally with the CSN (in this case, the catalytically-active JAB1 subunit), but this effect is not because the deleted amino acid sequence actually binds to JAB1. FHHt-causing Cul3 mutations lead to deletion of exon 9, which encodes the 4HB domain (Figure 1A). Min et al. (15) examined the CSN binding domain of a homologous cullin, cullin 1, and suggested that it lies within the 4HB domain. To determine whether the same domain is relevant in Cul3 binding to CSN, we mapped the Cul3 domains that are required for association with JAB1. Using multiple Cul3 constructs, we determined that the 4HB domain is neither necessary nor sufficient for CSN binding. Instead, the α/β_1 domain, which lies adjacent to the 4HB domain, was identified as essential for association with the CSN. Since the α/β_1 domain is not directly altered by the Cul3Δ403-459 mutation, the results suggest that the mutation disrupts binding to the CSN through alterations in the protein folding of Cul3; this suggestion aligns with the structural modeling data of Schumacher and colleagues (24).

Since Cul3Δ403-459 does not bind efficiently to JAB1 protein we tested whether JAB1 knockdown could mimic the effects of Cul3Δ403-459 in cultured cells. Knockdown of JAB1 with siRNA decreased, rather than increased, WNK4 protein abundance indicating increased CRL activity (Figure 2). This suggests that JAB1 knockdown alone cannot mimic Cul3Δ403-459 effects on WNK4; it should be noted, however, that CRL activity can differ between cell culture models and *in vivo*. The CSN positively regulates CRLs *in vivo* (22), whereas *in vitro* CRLs are negatively regulated by the CSN (36). Further, *in vivo*, experiments are needed to fully understand the effects of JAB1 inhibition.

The Cul3Δ403-459 K712R mutant prevented NEDD8 conjugation, effectively inhibiting ubiquitin ligase activity. However, Cul3Δ403-459 K712R, unexpectedly, still showed significant degradation of KLHL3 (Figure 4D), suggesting that degradation might be due to a non-ligase effect of the mutant Cul3Δ403-459. The results suggest that this ligase-independent degradation of KLHL3 occurs through the autophagy pathway, as two different inhibitors of this pathway, chloroquine, and 3-MA, both prevented KLHL3 degradation. Thus, as the schematic depicts in Figure 10, Cul3Δ403-459 facilitates KLHL3 degradation through two different pathways. KLHL3 is ubiquitylated and degraded via the proteasome. Additionally, KLHL3 can be degraded via selective autophagy, which is stimulated by the Cul3 mutant in a ligase-independent manner. Furthermore, the results here suggest that degradation of KLHL3 contributes importantly to WNK4 accumulation in FHHt. As shown, in the absence of WT-Cul3 (in HEK293T$^{Cul3\text{-}KO}$ cells), Cul3Δ403-459 cannot degrade WNK4, even when KLHL3 is abundant (Figure 7A). In cells that simultaneously express WT-Cul3 with Cul3Δ403-459, however, KLHL3 abundance proves limiting for WNK4 degradation (Figure 7B), and thus it is the ability of the mutant Cul3 to drive KLHL3 degradation that proves essential. These observations provide substantial insight into the mechanisms of the disease, which is characterized by the presence of one WT and one mutant Cul3 allele. In this case, the protein generated from Cul3Δ403-459 cannot degrade WNK4, creating functional haploinsufficiency, as suggested. Yet the ability of the WT-Cul3 protein to facilitate WNK kinase degradation

is limited by the low abundance of KLHL3; this is maintained by enhanced proteasomal- and autophagy-driven KLHL3 degradation (Figure 10).

The Cul3 mutation is contained within a protein that is a part the UPS, yet Cul3Δ403-459 causes an increase in autophagic degradation of KLHL3 (Figure 6B). The reason for this could be due to the relationship between the two degradative pathways. The UPS and autophagy were once thought to be separate mechanisms for regulated protein turnover, however, recent work has demonstrated that the two pathways may not be independent of one another. First, inhibition of the proteasome causes an increase in autophagy (8). This is most likely due to the fact that many proteins involved in the autophagy pathway are substrates for E3 ubiquitin ligases, including CRLs, and are negatively regulated via the UPS (7). Additionally, ubiquitylated proteins can be shuttled to the autophagophore (the vesicle that ultimately binds to the lysosome) via a linker protein, such as p62 (11). These proteins connect the two pathways by binding to both ubiquitylated proteins and autophagophore-membrane proteins allowing for ubiquitylated proteins to be degraded via autophagy. p62 binds to KLHL3 and mediates its degradation via autophagy when the proteasomal pathway is inhibited (16). Thus, the Cul3 mutation could lead to upregulation of p62-mediated autophagic degradation of KLHL3; moreover, the impairment of CRL substrate degradation, as shown with the Cul3 mutant, could cause activation of autophagy due to accumulation of CRL substrates that are critical for the process.

CRLs can associate with hundreds of substrate adaptors which can target thousands of substrates. Global deletion of the *Cul3* gene is embryonic lethal in mice (26). So, the fact that Cul3Δ403-459 doesn't produce widespread phenotypic effects has been perplexing. Here, we suggest that this paradox is resolved by dual effects of the Cul3Δ403-459 mutant protein, loss of function with respect to WNK4 degradation, and gain of function with respect to autophagocytic degradation of KLHL3. The latter effect likely contributes to the apparent tissue specificity for the disease to disrupt kidney and vascular smooth muscle. Although Cul3Δ403-459 avidly binds to and degrades KLHL3, its effects on other adaptor proteins are different. The substrate adaptors Bacurd1 and RhoBTB1 similarly showed higher levels of interaction with Cul3Δ403-459 compared to WT-Cul3 (10). Yet, Cul3Δ403-459 degraded RhoBTB1 less efficiently compared to WT-Cul3, and Bacurd1 showed no change in abundance. Here, Keap1, also known as Kelch-like 19, like Bacurd1, did not show a change in protein abundance due to Cul3Δ403-459 (Figure 9). Although Cul3Δ403-459 has differential effects on these substrate adaptors, the effects of Cul3Δ403-459 on their respective substrates were similar. Analogous to WNK4, the Bacurd1 substrate RhoA, which is expressed in the vascular smooth muscle and important for arterial pressure regulation, was upregulated by Cul3Δ403-459 (1). Additionally, as shown above, the Keap1 substrate and oxidative stress response protein, Nrf2, showed increased protein abundance (Figure 9). On the other hand, cyclin E, a protein involved in cell cycle regulation and a substrate of Cul3, was unaffected by Cul3Δ403-459. The data demonstrate that the altered structure of Cul3Δ403-459 may be sequestering adaptors in a manner that prevents normal ubiquitin ligase activity toward the substrate; yet KLHL3 may be one of only

a few adaptors that undergoes active degradation, providing specificity for tissues and cell types in which this protein is highly expressed.

All FHHt patients reported to date who harbor mutations in *Cul3* are heterozygous (4). Some have suggested that the Cul3Δ403-459 protein is unstable, leading to functional haploinsufficiency of the wild type protein; according to this model, individuals with one functional Cul3 allele should exhibit the phenotype (1, 24). Yet, Uchida and colleagues generated a mouse model that lacked one Cul3 allele, expressing approximately half as much Cul3 protein as control mice; the mice, however, did not show any evidence of the FHHt phenotype (2). Further, Ferdaus and colleagues (9) recently showed that mice with one Cul3 allele also lack features of FHHt, whereas mice with one mutant and one wild type allele exhibit frank hyperkalemic hypertension. While the protein derived from Cul3Δ403-459 does appear to be unstable, *in vivo* (1, 24), the current results suggest that the FHHt phenotype requires a second, dominant-negative effect. In support of this, we found clear evidence for a dominant effect of Cul3Δ403-459 on Cul3 WT, when the ratio of WT to mutant construct was varied (Figure 8). This is largely consistent with the model suggested by Sigmund and colleagues, who found that Cul3Δ403-459 exhibited enhanced interaction with substrate adaptors, such as KLHL3, and suggested that the mutant cullin might act in a dominant manner, despite reduced abundance, by sequestering adaptor proteins (10).

The results here show only a modest change in WNK4 when WT Cul3 and Cul3Δ403-459 are transfected together, and increasing the ratio of WT Cul3 to Cul3Δ403-459 further diminished the effects on WNK4 abundance. This raises questions about the direct relevance of this to the human disease, as all FHHt patients are heterozygous, with one WT and one mutant allele. Additionally, in experimental disease models, the abundance of Cul3Δ403-459 is very low, relative to the wild type allele. Yet, Ferdaus and colleagues (9) showed recently that Cul3Δ403-459 exerts dominant effects, *in vivo*, despite its low abundance. Thus, these limitations of using HEK293 cells imply that these hypotheses should be explored using physiologically more relevant model systems.

Thus, the current results clarify the consequences of deletion of exon 9 in *Cul3*, and provide novel information about how Cul3 interacts with the CSN. They suggest that this interaction requires the α/β_1 domain, which lies next to, but is distinct from, the 4HB domain deleted in the human disease. Thus, although the deletion impairs binding of Cul3 to the CSN, the deleted region itself does not mediate the association. Furthermore, the results stress the importance of KLHL3 in the regulation of WNK4. Our data would be consistent with an effect of the mutant Cul3 protein to bind avidly to specific substrate adaptors, forming unstable and ineffective complexes. Additional studies will be required to further evaluate this hypothesis.

Author Contributions

R.J. Cornelius, C. Zhang, J.D. Singer, C. Yang, and D.H. Ellison designed research. R.J. Cornelius, C. Zhang, and K.J. Erspamer performed research. L.N. Agbor and C.D. Sigmund generated HEK293T$^{Cul3\text{-}KO}$ cells. R.J. Cornelius, C. Zhang, K.J. Erspamer, J.D. Singer, C. Yang, and D.H. Ellison analyzed data. R.J Cornelius and D.H. Ellison wrote the paper. R.J. Cornelius, C. Zhang, K.J. Erspamer, L.N. Agbor, C.D. Sigmund, J.D. Singer, C. Yang, and D.H. Ellison edited the paper.

Acknowledgements

We thank James McCormick for the helpful discussions.

Grants

This work was supported by NIH grants R01 DK51496 (D.H. Ellison and C. Yang) and T32 DK067864 (D.H. Ellison), as well as by Merit Review grant 1I01BX002228-01A1 from the Department of Veteran Affairs (D.H. Ellison), and by AHA 16POST3064003 and NIH F32 DK112531 (R.J. Cornelius). C. Zhang was supported by the National Natural Science Foundation of China 81570634 and 81770706. C.D. Sigmund was supported by NIH grant R01 HL125603.

Disclosures

The authors declare that they have no conflicts of interest.

References

1. **Agbor LN**, **Ibeawuchi S-RC**, **Hu C**, **Wu J**, **Davis DR**, **Keen HL**, **Quelle FW**, **Sigmund CD**. Cullin-3 mutation causes arterial stiffness and hypertension through a vascular smooth muscle mechanism. *JCI insight* 1: e91015, 2016.

2. **Araki Y**, **Rai T**, **Sohara E**, **Mori T**, **Inoue Y**, **Isobe K**, **Kikuchi E**, **Ohta A**, **Sasaki S**, **Uchida S**. Generation and analysis of knock-in mice carrying pseudohypoaldosteronism type II-causing mutations in the cullin 3 gene. *Biol Open* 4: 1509–17, 2015.

3. **Boh BK**, **Smith PG**, **Hagen T**. Neddylation-Induced Conformational Control Regulates Cullin RING Ligase Activity In Vivo. *J Mol Biol* 409: 136–145, 2011.

4. **Boyden LM**, **Choi M**, **Choate KA**, **Nelson-Williams CJ**, **Farhi A**, **Toka HR**, **Tikhonova IR**, **Bjornson R**, **Mane SM**, **Colussi G**, **Lebel M**, **Gordon RD**, **Semmekrot BA**, **Poujol A**, **Välimäki MJ**, **De Ferrari ME**, **Sanjad SA**, **Gutkin M**, **Karet FE**, **Tucci JR**, **Stockigt JR**, **Keppler-Noreuil KM**, **Porter CC**, **Anand SK**, **Whiteford ML**, **Davis ID**, **Dewar SB**, **Bettinelli A**, **Fadrowski JJ**, **Belsha CW**, **Hunley TE**, **Nelson RD**, **Trachtman H**, **Cole TRP**, **Pinsk M**, **Bockenhauer D**, **Shenoy M**, **Vaidyanathan P**, **Foreman JW**, **Rasoulpour M**, **Thameem F**, **Al-Shahrouri HZ**, **Radhakrishnan J**, **Gharavi AG**, **Goilav B**, **Lifton RP**. Mutations in kelch-like 3 and cullin 3 cause hypertension and electrolyte abnormalities. *Nature* 482: 98–102, 2012.

5. **Cavadini S**, **Fischer ES**, **Bunker RD**, **Potenza A**, **Lingaraju GM**, **Goldie KN**, **Mohamed WI**, **Faty M**, **Petzold G**, **Beckwith REJ**, **Tichkule RB**, **Hassiepen U**, **Abdulrahman W**, **Pantelic RS**, **Matsumoto S**, **Sugasawa K**, **Stahlberg H**, **Thomä NH**. Cullin–RING ubiquitin E3 ligase regulation by the COP9 signalosome. *Nature* 531: 598–603, 2016.

6. **Chung D**, **Dellaire G**. The Role of the COP9 Signalosome and Neddylation in DNA Damage Signaling and Repair. *Biomolecules* 5: 2388–2416, 2015.

7. **Cui D**, **Xiong X**, **Zhao Y**. Cullin-RING ligases in regulation of autophagy. *Cell Div* 11: 8, 2016.

8. **Ding W-X**, **Ni H-M**, **Gao W**, **Yoshimori T**, **Stolz DB**, **Ron D**, **Yin X-M**. Linking of Autophagy to Ubiquitin-Proteasome System Is Important for the Regulation of Endoplasmic Reticulum Stress and Cell Viability. *Am J Pathol* 171: 513–524, 2007.

9. **Ferdaus MZ**, **Miller LN**, **Agbor LN**, **Saritas T**, **Singer JD**, **Sigmund CD**, **McCormick JA**. Mutant Cullin 3 causes familial hyperkalemic hypertension via dominant effects. *JCI Insight* 2, 2017.

10. **Ibeawuchi SC**, **Agbor LN**, **Quelle FW**, **Sigmund CD**. Hypertension Causing Mutations in Cullin3 Impair RhoA Ubiquitination and Augment Association with Substrate Adaptors. *J Biol Chem* 290: 19208–19217, 2015.

11. **Korolchuk VI**, **Menzies FM**, **Rubinsztein DC**. Mechanisms of cross-talk between the ubiquitin-proteasome and autophagy-lysosome systems. *FEBS Lett* 584: 1393–1398, 2010.

12. **Lingaraju GM**, **Bunker RD**, **Cavadini S**, **Hess D**, **Hassiepen U**, **Renatus M**, **Fischer ES**, **Thomä NH**. Crystal structure of the human COP9 signalosome. *Nature* 512: 161–5, 2014.

13. **Mayan H**, **Vered I**, **Mouallem M**, **Tzadok-Witkon M**, **Pauzner R**, **Farfel Z**. Pseudohypoaldosteronism type II: marked sensitivity to thiazides, hypercalciuria, normomagnesemia, and low bone mineral density. *J Clin Endocrinol Metab* 87: 3248–54, 2002.

14. **McCormick JA**, **Yang C-L**, **Zhang C**, **Davidge B**, **Blankenstein KI**, **Terker AS**, **Yarbrough B**, **Meermeier NP**, **Park HJ**, **McCully B**, **West M**, **Borschewski A**, **Himmerkus N**, **Bleich M**, **Bachmann S**, **Mutig K**, **Argaiz ER**, **Gamba G**, **Singer JD**, **Ellison DH**. Hyperkalemic hypertension–associated cullin 3 promotes WNK signaling by degrading KLHL3. *J Clin Invest* 124: 4723–4736, 2014.

15. **Min KW**, **Kwon MJ**, **Park HS**, **Park Y**, **Sungjoo KY**, **Yoon JB**. CAND1 enhances deneddylation of CUL1 by COP9 signalosome. *Biochem Biophys Res Commun* 334: 867–874, 2005.

16. **Mori Y**, **Mori T**, **Wakabayashi M**, **Yoshizaki Y**, **Zeniya M**, **Sohara E**, **Rai T**, **Uchida S**. Involvement of selective autophagy mediated by p62/SQSTM1 in KLHL3-dependent WNK4 degradation. *Biochem J* 472: 33–41, 2015.

17. **Mori Y**, **Wakabayashi M**, **Mori T**, **Araki Y**, **Sohara E**, **Rai T**, **Sasaki S**, **Uchida S**. Decrease of WNK4 ubiquitination by disease-causing mutations of KLHL3 through different molecular mechanisms. *Biochem Biophys Res Commun* 439: 30–34, 2013.

18. **Ohta A**, **Schumacher F-R**, **Mehellou Y**, **Johnson C**, **Knebel A**, **Macartney TJ**, **Wood NT**, **Alessi DR**, **Kurz T**. The CUL3-KLHL3 E3 ligase complex mutated in Gordon's hypertension syndrome interacts with and ubiquitylates WNK isoforms: disease-causing mutations in KLHL3 and WNK4 disrupt interaction. *Biochem J* 451: 111–22, 2013.

19. **Pacheco-Alvarez D**, **Cristóbal PS**, **Meade P**, **Moreno E**, **Vazquez N**, **Muñoz E**, **Díaz A**, **Juárez ME**, **Giménez I**, **Gamba G**. The Na+:Cl- cotransporter is activated and phosphorylated at the amino-terminal domain upon intracellular chloride depletion. *J Biol Chem* 281: 28755–63, 2006.

20. **Pan Z-Q**, **Kentsis A**, **Dias DC**, **Yamoah K**, **Wu K**. Nedd8 on cullin: building an expressway to protein destruction. *Oncogene* 23: 1985–1997, 2004.

21. **Pathare G**, **Hoenderop JGJ**, **Bindels RJM**, **San-Cristobal P**. A molecular update on pseudohypoaldosteronism type II. *Am J Physiol Renal Physiol* 305: F1513-20, 2013.

22. **Pintard L**, **Kurz T**, **Glaser S**, **Willis JH**, **Peter M**, **Bowerman B**. Neddylation and deneddylation of

CUL-3 is required to target MEI-1/Katanin for degradation at the meiosis-to-mitosis transition in C. elegans. *Curr Biol* 13: 911–21, 2003.

23. **Saha A**, **Deshaies RJ**. Multimodal Activation of the Ubiquitin Ligase SCF by Nedd8 Conjugation. *Mol Cell* 32: 21–31, 2008.

24. **Schumacher F-R**, **Siew K**, **Zhang J**, **Johnson C**, **Wood N**, **Cleary SE**, **Al Maskari RS**, **Ferryman JT**, **Hardege I**, **Yasmin**, **Figg NL**, **Enchev R**, **Knebel A**, **O'Shaughnessy KM**, **Kurz T**. Characterisation of the Cullin-3 mutation that causes a severe form of familial hypertension and hyperkalaemia. *EMBO Mol Med* 7: 1285–306, 2015.

25. **Shibata S**, **Zhang J**, **Puthumana J**, **Stone KL**, **Lifton RP**. Kelch-like 3 and Cullin 3 regulate electrolyte homeostasis via ubiquitination and degradation of WNK4. *Proc Natl Acad Sci U S A* 110: 7838–43, 2013.

26. **Singer JD**, **Gurian-West M**, **Clurman B**, **Roberts JM**. Cullin-3 targets cyclin E for ubiquitination and controls S phase in mammalian cells. *Genes Dev* 13: 2375–87, 1999.

27. **Sohara E**, **Uchida S**. Kelch-like 3/Cullin 3 ubiquitin ligase complex and WNK signaling in salt-sensitive hypertension and electrolyte disorder. *Nephrol Dial Transplant* 31: 1417–1424, 2016.

28. **Susa K**, **Sohara E**, **Rai T**, **Zeniya M**, **Mori Y**, **Mori T**, **Chiga M**, **Nomura N**, **Nishida H**, **Takahashi D**, **Isobe K**, **Inoue Y**, **Takeishi K**, **Takeda N**, **Sasaki S**, **Uchida S**. Impaired degradation of WNK1 and WNK4 kinases causes PHAII in mutant KLHL3 knock-in mice. *Hum Mol Genet* 23: 5052–60, 2014.

29. **Vidal-Petiot E**, **Elvira-Matelot E**, **Mutig K**, **Soukaseum C**, **Baudrie V**, **Wu S**, **Cheval L**, **Huc E**, **Cambillau M**, **Bachmann S**, **Doucet A**, **Jeunemaitre X**, **Hadchouel J**. WNK1-related Familial Hyperkalemic Hypertension results from an increased expression of L-WNK1 specifically in the distal nephron. *Proc Natl Acad Sci U S A* 110: 14366–71, 2013.

30. **Vitari AC**, **Deak M**, **Morrice NA**, **Alessi DR**. The WNK1 and WNK4 protein kinases that are mutated in Gordon's hypertension syndrome phosphorylate and activate SPAK and OSR1 protein kinases. *Biochem J* 391: 17–24, 2005.

31. **Wakabayashi M**, **Mori T**, **Isobe K**, **Sohara E**, **Susa K**, **Araki Y**, **Chiga M**, **Kikuchi E**, **Nomura N**, **Mori Y**, **Matsuo H**, **Murata T**, **Nomura S**, **Asano T**, **Kawaguchi H**, **Nonoyama S**, **Rai T**, **Sasaki S**, **Uchida S**. Impaired KLHL3-mediated ubiquitination of WNK4 causes human hypertension. *Cell Rep* 3: 858–868, 2013.

32. **Wilson FH**, **Disse-Nicodème S**, **Choate KA**, **Ishikawa K**, **Nelson-Williams C**, **Desitter I**, **Gunel M**, **Milford D V**, **Lipkin GW**, **Achard JM**, **Feely MP**, **Dussol B**, **Berland Y**, **Unwin RJ**, **Mayan H**, **Simon DB**, **Farfel Z**, **Jeunemaitre X**, **Lifton RP**. Human hypertension caused by mutations in WNK

kinases. *Science* 293: 1107–12, 2001.

33. **Wimuttisuk W**, **Singer JD**. The Cullin3 ubiquitin ligase functions as a Nedd8-bound heterodimer. *Mol Biol Cell* 18: 899–909, 2007.

34. **Wu G**, **Peng J-B**. Disease-causing mutations in KLHL3 impair its effect on WNK4 degradation. *FEBS Lett* 587: 1717–1722, 2013.

35. **Wu J-T**, **Lin H-C**, **Hu Y-C**, **Chien C-T**. Neddylation and deneddylation regulate Cul1 and Cul3 protein accumulation. *Nat Cell Biol* 7: 1014–1020, 2005.

36. **Yang X**, **Menon S**, **Lykke-Andersen K**, **Tsuge T**, **Di Xiao**, **Wang X**, **Rodriguez-Suarez RJ**, **Zhang H**, **Wei N**. The COP9 signalosome inhibits p27(kip1) degradation and impedes G1-S phase progression via deneddylation of SCF Cul1. *Curr Biol* 12: 667–72, 2002.

37. **Yewdell JW**, **Lacsina JR**, **Rechsteiner MC**, **Nicchitta C V**. Out with the old, in with the new? Comparing methods for measuring protein degradation. *Cell Biol Int* 35: 457–62, 2011.

Figure Legends

Figure 1. CSN binds to Cul3 at the α/β_1 domain. A) Diagram of Cul3 domain structure and schematic of the Cul3 constructs. B) Co-immunoprecipitation was performed with HEK293 cells transfected with myc-JAB1 and FLAG-tagged WT-Cul3 or Cul3Δ403-459 and analyzed by immunoblot. Cul3Δ403-459 exhibited a decreased interaction with JAB1 compared to WT-Cul3. C) The effects of Cul3Δ403-459 on JAB1 binding was determined by co-immunoprecipitation with N-terminal domain Cul3 constructs using anti-FLAG and analyzed by immunoblot. Co-immunoprecipitation of N-terminal domain Cul3 constructs with (1-459) and without (1-402) the 4HB domain showed no binding to JAB1. D) Segments of the Cul3 protein were generated with a GST tag and co-transfected with myc-tagged JAB1. Co-immunoprecipitation was performed using glutathione sepharose beads. Immunoblotting for JAB1 showed binding to 4HB:α/β_1 and α/β_1 Cul3 constructs, but not to 4HB, WH-A:α/β:WH-B, or R1:R2:R3 Cul3 constructs. E) Co-immunoprecipitation was performed with myc-JAB1 and FLAG-tagged WT-Cul3 or Cul3Δ461-586 constructs. Cul3Δ461-586 demonstrated less binding to JAB1 protein compared to WT-Cul3. Immunoblotting for NEDD8 showed enhanced neddylation of the Cul3Δ461-586 construct compared to WT-Cul3. The *asterisk* indicates a nonspecific band.

Figure 2. Effects of JAB1 inhibition on Cul3 neddylation and substrate protein abundance. Myc-tagged KLHL3 or WNK4 was co-transfected into HEK293 cells with either JAB1 siRNA or control siRNA. The proteins were examined by immunoblot in cells with endogenous WT-Cul3. JAB1 siRNA decreased JAB1, KLHL3, and WNK4 abundance, increased NEDD8 abundance, and the neddylated form of Cul3 (top band). β-actin was used as a loading control.

Figure 3. Cul3Δ403-459 decreases the stability of KLHL3. A. Cycloheximide chase assay was performed with HEK293 cells co-transfected with myc-tagged KLHL3 and either FLAG-WT Cul3 or FLAG-Cul3Δ403-459. Due to a robust decrease in KLHL3 by the Cul3Δ403-459 which prevented quantification, the amount of Cul3Δ403-459 transfected was reduced to half of WT Cul3. Cycloheximide (100 μg/ml) was added 36 h post transfection and cells were lysed at 0, 1, 2, 4, 8, and 24 h time points. KLHL3 protein abundance was more rapidly degraded in cells co-expressing Cul3Δ403-459. Right, quantitative analysis of KLHL3 protein abundance. Stain-free imaging was used as a loading control. Linear regression was used to determine the slope of each group. The differences between the slopes were significantly different ($P < 0.001$). Data represent mean values ± SEM relative to the 0 h time point. Statistical differences were examined using two-tailed unpaired Student's t test. * $P = 0.01$ vs WT. B. Cycloheximide chase assay was performed with HEK293 cells co-transfected with myc-tagged WNK4 in the presence or absence of KLHL3. Cycloheximide (100 μg/ml) was added 36 h post transfection and cells were lysed at 0, 2, 4, and 6 h time points. Stain-free imaging was used as a loading control. C. Left, quantitative analysis of KLHL3; all data points are relative to WT Cul3 0 h time point.

Right, quantitative analysis of WNK4 protein abundance; all data points are relative to WNK4 without KLHL3 0 h time point. The effects of Cul3Δ403-459 on KLHL3 abundance is similar to the effects of KLHL3 on WNK4 abundance.

Figure 4. Ligase-deficient Cul3Δ403-459 K712R double mutant blunts the effects of Cul3Δ403-459 on KLHL3 and WNK4. A) FLAG-tagged Cul3 constructs were co-transfected into HEK293 cells and immunoprecipitated using FLAG antibody. Immunoblotting for NEDD8 showed no neddylation of the K712R mutant for both WT-Cul3 and Cul3Δ403-459. B) Co-immunoprecipitation was performed with HEK293 cells transfected with myc-KLHL3 and FLAG-tagged WT-Cul3, Cul3Δ403-459, Cul3Δ403-459 K712R, or empty vector. Pull-down with FLAG antibodies showed that KLHL3 had more binding to Cul3Δ403-459 and Cul3Δ403-459 K712R proteins. C) A ubiquitin assay was performed for KLHL3 by co-transfecting FLAG-tagged Cul3 constructs with myc-KLHL3 and HA-tagged ubiquitin. Immunoprecipitation was performed using anti-myc antibody and poly-ubiquitylation of KLHL3 was visualized by immunoblotting for anti-HA. Cul3Δ403-459 K712R double mutant attenuated the higher abundance of KLHL3 ubiquitylation shown with Cul3Δ403-459. D) Top, abundance of myc-tagged KLHL3 and WNK4 protein was examined by immunoblot in HEK293T$^{Cul3\text{-}KO}$ cells co-transfected with different FLAG-tagged Cul3 constructs. KLHL3 and WNK4 expression was higher and lower, respectively, in Cul3Δ403-459 K712R compared to Cul3Δ403-459. Bottom, quantitative analysis of KLHL3 and WNK4 protein abundance. Stain-free imaging was used as a loading control. Data represent individual values as well as mean ± SEM relative to control. Statistical differences were examined by one-way ANOVA with Tukey's post hoc analysis.

Figure 5. Effects of proteasome inhibition on Cul3Δ403-459-mediated KLHL3 degradation. The pathway for degradation **of** KLHL3 by the Cul3Δ403-459 mutant was examined by inhibiting the proteasomal pathway with the drug MG132. HEK293 cells were co-transfected with myc-KLHL3 and either no Cul3 or FLAG-Cul3Δ403-459. The cells were incubated with vehicle or 10 μM MG132 for 18 hours before harvesting. Immunoblot analysis showed that inhibition of the proteasomal pathway partially blocked Cul3Δ403-459-mediated KLHL3 degradation. Right, quantitative analysis of KLHL3 protein abundance. GAPDH was used as a loading control. Data represent individual values as well as mean ± SEM relative to control. Statistical differences were examined by one-way ANOVA with Tukey's post hoc analysis.

Figure 6. Effects of autophagy inhibition on Cul3Δ403-459-mediated KLHL3 degradation. The pathway for degradation of KLHL3 by the Cul3Δ403-459 mutant was examined by inhibiting the autophagy pathway with the drugs chloroquine or 3-methyladenine (3-MA). HEK293 cells were co-transfected with myc-KLHL3 and either no Cul3 or FLAG-Cul3Δ403-459. The cells were incubated with vehicle or 100 μM chloroquine (A), or 5 mM 3-MA (C) for 18 hours before harvesting. Immunoblot analysis

showed that inhibition of autophagy with chloroquine or 3-MA partially blocked Cul3Δ403-459-mediated KLHL3 degradation, while administration of the drugs together completely eliminated KLHL3 degradation. Right, quantitative analysis of KLHL3 protein abundance. B) Bar graph depicting the percent change in KLHL3 protein abundance caused by autophagy inhibition from chloroquine administration between control and Cul3Δ403-459 groups. D) Cells were incubated with both the proteasomal inhibitor MG132 and autophagy inhibitor chloroquine simultaneously. Administration of the drugs together completely eliminated KLHL3 degradation. GAPDH was used as a loading control. Data represent individual values as well as mean ± SEM relative to control. Statistical differences were examined by one-way ANOVA with Tukey's post hoc analysis.

Figure 7. Increased expression of KLHL3 can overcome effects of Cul3Δ403-459 on WNK4 in the presence of WT-Cul3. HEK293T$^{Cul3\text{-}KO}$ cells (A) or HEK293 cells (B) were transfected with myc-WNK4 and either FLAG-tagged WT-Cul3 or Cul3Δ403-459 along with increasing amounts of myc-tagged KLHL3 and analyzed by immunoblot. The increased KLHL3 expression only slightly decreased WNK4 protein abundance in HEK293T$^{Cul3\text{-}KO}$ cells, however, HEK293 cells had a larger decrease in WNK4 which was not significantly different from WT-Cul3. Bar graphs depict quantification of KLHL3 and WNK4 protein abundance. Stain-free imaging was used as a loading control. Data represent relative individual values as well as mean ± SEM. Statistical differences were examined by one-way ANOVA with Tukey's post hoc analysis.

Figure 8. WT-Cul3 and Cul3Δ403-459 compete for KLHL3. Myc-tagged KLHL3 and WNK4 were co-transfected with different amounts of FLAG-tagged WT-Cul3 and Cul3Δ403-459. The ratio of FLAG-WT-Cul3 to Cul3Δ403-459 was adjusted as labeled and analyzed by immunoblot. β-actin was used as a loading control. Increasing the ratio of Cul3Δ403-459 to WT-Cul3 decreased KLHL3 and increased WNK4 protein expression. The opposite was observed when increasing the ratio of WT-Cul3 to Cul3Δ403-459. Bar graphs are a summary of the densitometry analysis of the blot.

Figure 9. Effects of Cul3Δ403-459 on Keap1, Nrf2, and cyclin E. Top, abundance of endogenous Keap1, Nrf2, and cyclin E protein was examined in HEK293T$^{Cul3\text{-}KO}$ cells co-transfected with different FLAG-tagged Cul3 constructs and analyzed by immunoblot. Keap1 and cyclin E showed no difference in protein abundance between the groups. Nrf2 protein levels were higher in Cul3Δ403-459 and Cul3Δ403-459 K712R transfected cells. Stain-free imaging was used as a loading control. Bottom, quantitative analysis of Keap1, Nrf2, and cyclin E protein abundance. Data represent relative individual values as well as mean ± SEM. Statistical differences were examined by one-way ANOVA with Tukey's post hoc analysis.

Figure 10. Simplified model of Cul3Δ403-459 effects on KLHL3 and WNK4. KLHL3 is degraded by two separate pathways. Under normal conditions, the WT-Cul3-KLHL3 ubiquitin ligase complex (left) ubiquitylates WNK4 targeting it for degradation via the proteasome. Separate from cullin-RING-ligase activity, KLHL3 is also degraded through selective autophagy. The Cul3Δ403-459 FHHt mutant (right) targets KLHL3 instead of WNK4 for ubiquitylation; causing proteasomal degradation of KLHL3 while preventing WNK4 turnover. Additionally, expression of the Cul3 mutant causes enhanced autophagic-mediated degradation of KLHL3. The lower levels of KLHL3 through both proteasomal and autophagic degradation prevent WT-Cul3 from interacting with WNK4, leading to an increase in WNK4 protein abundance.

Table 1. Antibodies used for Western blot

Figure	Target	Antibody Name	Source	1° Dilution	2° Dilution
1E,2	JAB1	JAB1 FL-334	Santa Cruz, SC-9074	1:1,000, 1h at RT	1:5,000
1C,1D	JAB1	JAB1 6C3.38	Thermo Scientific	1:2,000, 1h at RT	1:5,000
1D	GST	GST B-14	Santa Cruz, SC-138	1:1,000, 1h at RT	1:2,500
1,2,3,4,5,6,7,8	Myc	c-Myc	Sigma Aldrich, M5546	1:5,000, 1h at RT	1:10,000
1E,2,4A	NEDD8	NEDD8 19E3	Cell Signaling 2754	1:1,000, o/n at 4°C	1:2,500
2,4D	Cul3	Cul3	Cell Signaling 2759	1:1,000, o/n at 4°C	1:2,500
2,8	β-actin	β-actin	Abcam Ab8227	1:5,000, 1h at RT	1:2,500
1,4,5,6,7,8,9	FLAG	FLAG M2	Sigma Aldrich, F3165	1:10,000, 1h at RT	1:10,000
4C	HA	HA.11	Covance MMS-101P	1:1,000, 1h at RT	1:10,000
5,6	GAPDH	GAPDH	Santa Cruz, SC-20357	1:1,000, 1h at RT	1:2,500
9	Keap1	Keap1	Abcam Ab139729	1:1,000, o/n at 4°C	1:2,500
9	Nrf2	Nrf2 H-300	Santa Cruz, SC-13032	1:1,000, o/n at 4°C	1:2,500
9	Cyclin E	Cyclin E HE12	Santa Cruz, SC-247	1:1,000, o/n at 4°C	1:2,500

Abbreviations: App, application; RT, room temperature; o/n, overnight; JAB1, jun activation domain-binding protein-1; GST, glutathione S-transferase; NEDD8, neuronal precursor cell expressed developmentally down-regulated protein 8; Cul3, cullin 3; Keap1, kelch-like ECH-associated protein 1; Nrf2, nuclear factor erythroid 2-related factor 2.

Figure 1

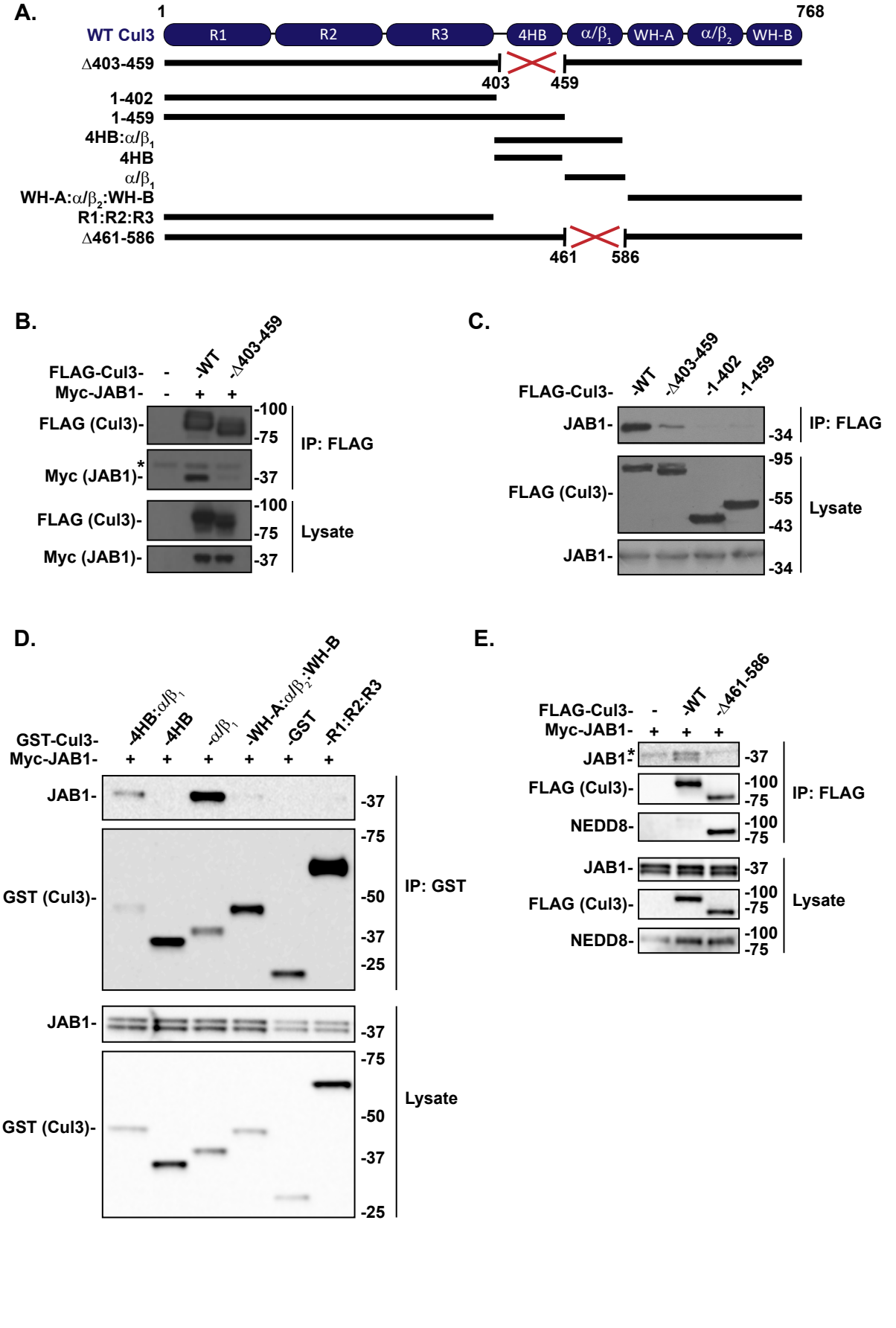
A.
1
768
WT Cul3
R1
R2
R3
4HB
α/β1
WH-A
α/β2
WH-B
Δ403-459
403
459
1-402
1-459
4HB:α/β1
4HB
α/β1
WH-A:α/β2:WH-B
R1:R2:R3
Δ461-586
461
586
B.
FLAG-Cul3- - -WT -Δ403-459
Myc-JAB1- - + +
FLAG (Cul3)-
Myc (JAB1)*-
IP: FLAG
FLAG (Cul3)-
Myc (JAB1)-
Lysate
-100
-75
-37
C.
FLAG-Cul3- -WT -Δ403-459 -1-402 -1-459
JAB1-
IP: FLAG
FLAG (Cul3)-
JAB1-
Lysate
-34
-95
-55
-43
D.
GST-Cul3- -4HB:α/β1 -4HB -α/β1 -WH-A:α/β2:WH-B -GST -R1:R2:R3
Myc-JAB1- + + + + + +
JAB1-
GST (Cul3)-
IP: GST
JAB1-
GST (Cul3)-
Lysate
-37
-75
-50
-25
E.
FLAG-Cul3- - -WT -Δ461-586
Myc-JAB1- + + +
JAB1*-
FLAG (Cul3)-
NEDD8-
IP: FLAG
JAB1-
FLAG (Cul3)-
NEDD8-
Lysate
-37
-100
-75

Figure 2

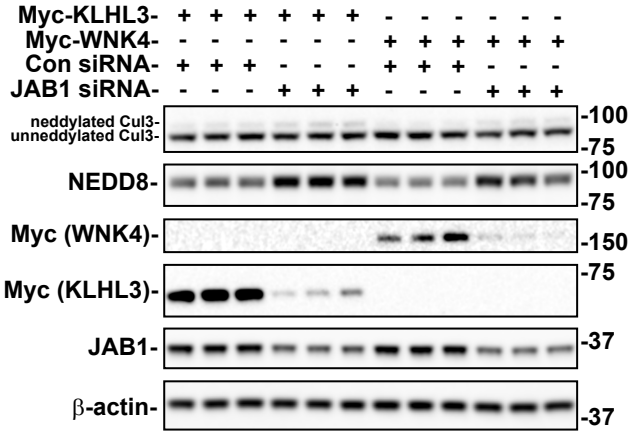
Myc-KLHL3- + + + + + + - - - - - -
Myc-WNK4- - - - - - - + + + + + +
Con siRNA- + + + - - - + + + - - -
JAB1 siRNA- - - - + + + - - - + + +
neddylated Cul3-
unneddylated Cul3-
-100
-75
NEDD8-
-100
-75
Myc (WNK4)-
-150
Myc (KLHL3)-
-75
JAB1-
-37
β-actin-
-37

Figure 3

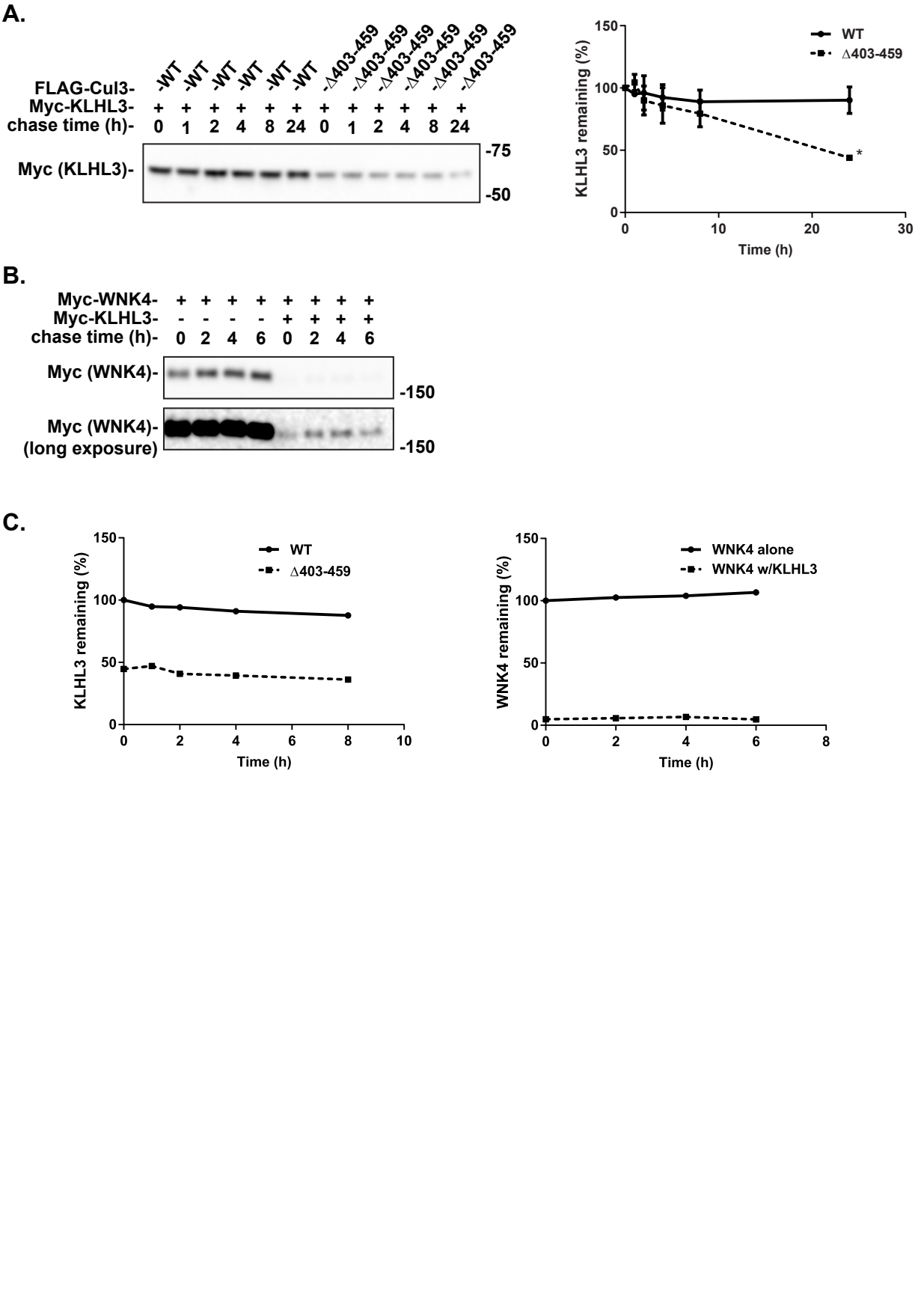
A.
FLAG-Cul3-
Myc-KLHL3-
chase time (h)-
-WT -WT -WT -WT -WT -WT
-Δ403-459 -Δ403-459 -Δ403-459 -Δ403-459 -Δ403-459 -Δ403-459
+ + + + + + + + + + + +
0 1 2 4 8 24 0 1 2 4 8 24
Myc (KLHL3)-
-75
-50
KLHL3 remaining (%)
WT
Δ403-459
*
Time (h)
B.
Myc-WNK4- + + + + + + + +
Myc-KLHL3- - - - - + + + +
chase time (h)- 0 2 4 6 0 2 4 6
Myc (WNK4)-
-150
Myc (WNK4)-
(long exposure)
-150
C.
KLHL3 remaining (%)
WT
Δ403-459
Time (h)
WNK4 remaining (%)
WNK4 alone
WNK4 w/KLHL3
Time (h)

Figure 4

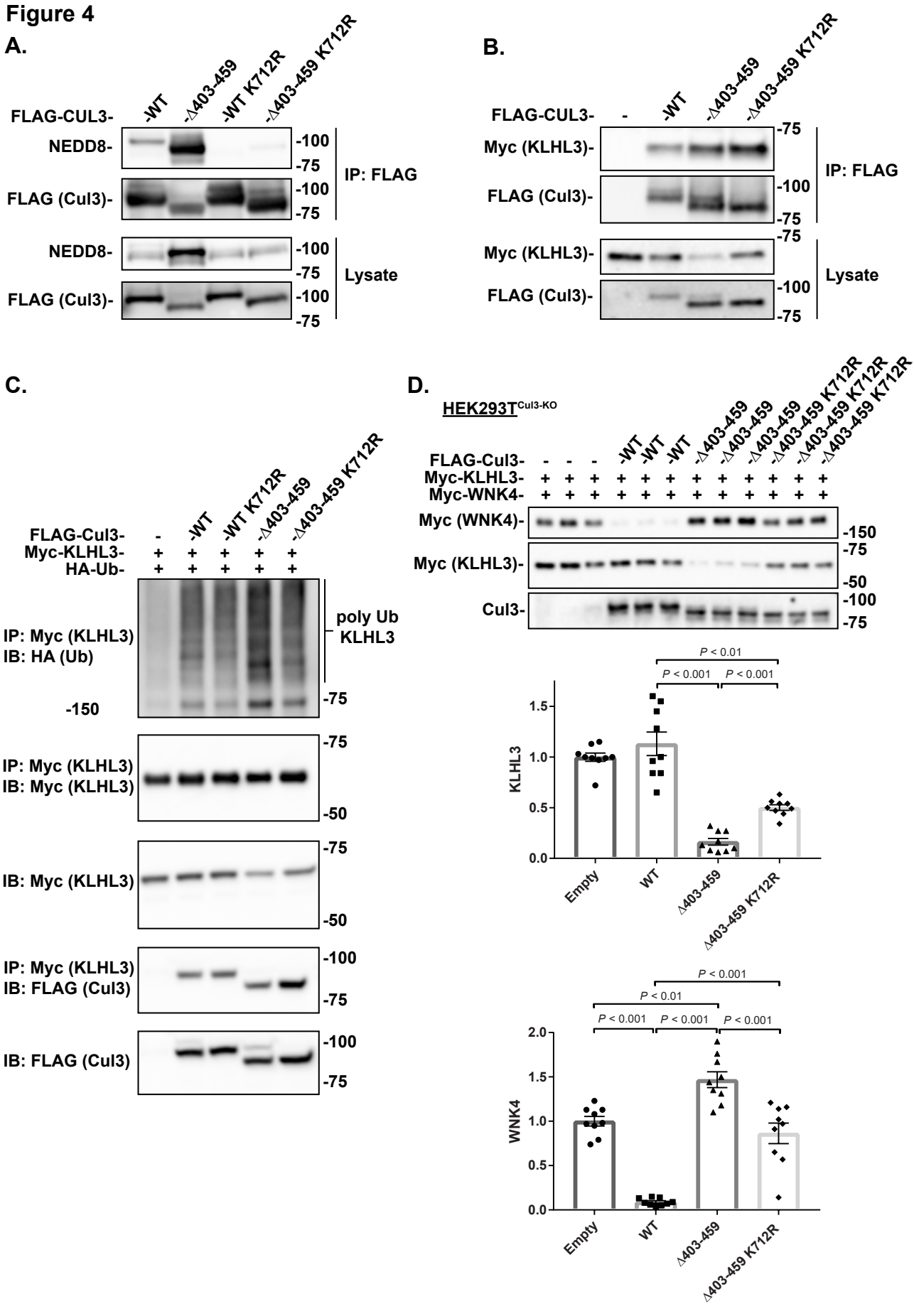
A.
FLAG-CUL3-
-WT
-Δ403-459
-WT K712R
-Δ403-459 K712R
NEDD8-
FLAG (Cul3)-
IP: FLAG
Lysate
-100
-75
B.
FLAG-CUL3-
-
-WT
-Δ403-459
-Δ403-459 K712R
Myc (KLHL3)-
FLAG (Cul3)-
IP: FLAG
Lysate
-75
-100
C.
FLAG-Cul3-
Myc-KLHL3-
HA-Ub-
IP: Myc (KLHL3)
IB: HA (Ub)
poly Ub KLHL3
-150
IP: Myc (KLHL3)
IB: Myc (KLHL3)
-50
IB: Myc (KLHL3)
IP: Myc (KLHL3)
IB: FLAG (Cul3)
IB: FLAG (Cul3)
D.
HEK293T Cul3-KO
Myc-WNK4-
Myc (WNK4)-
Myc (KLHL3)-
Cul3-
-150
P < 0.01
P < 0.001
KLHL3
1.5
1.0
0.5
0.0
Empty
WT
Δ403-459
Δ403-459 K712R
WNK4
2.0

Figure 5

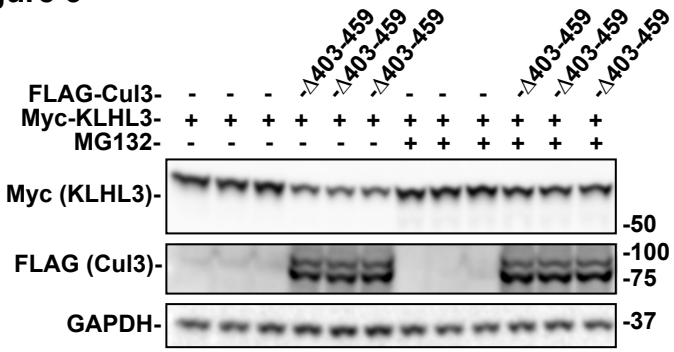
FLAG-Cul3- - - - -Δ403-459 -Δ403-459 -Δ403-459 - - - -Δ403-459 -Δ403-459 -Δ403-459
Myc-KLHL3- + + + + + + + + + + + +
MG132- - - - - - - + + + + + +
Myc (KLHL3)-
FLAG (Cul3)-
GAPDH-
-50
-100
-75
-37

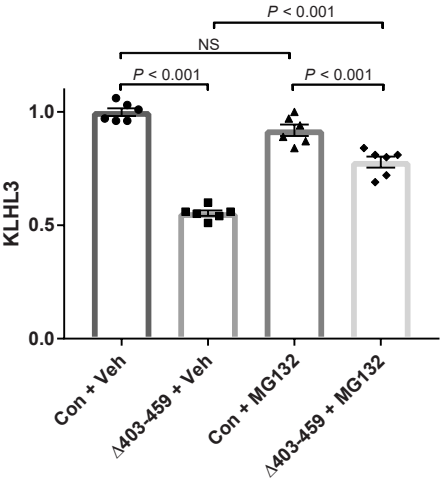
P < 0.001
NS
P < 0.001
P < 0.001
KLHL3
1.0
0.5
0.0
Con + Veh
Δ403-459 + Veh
Con + MG132
Δ403-459 + MG132

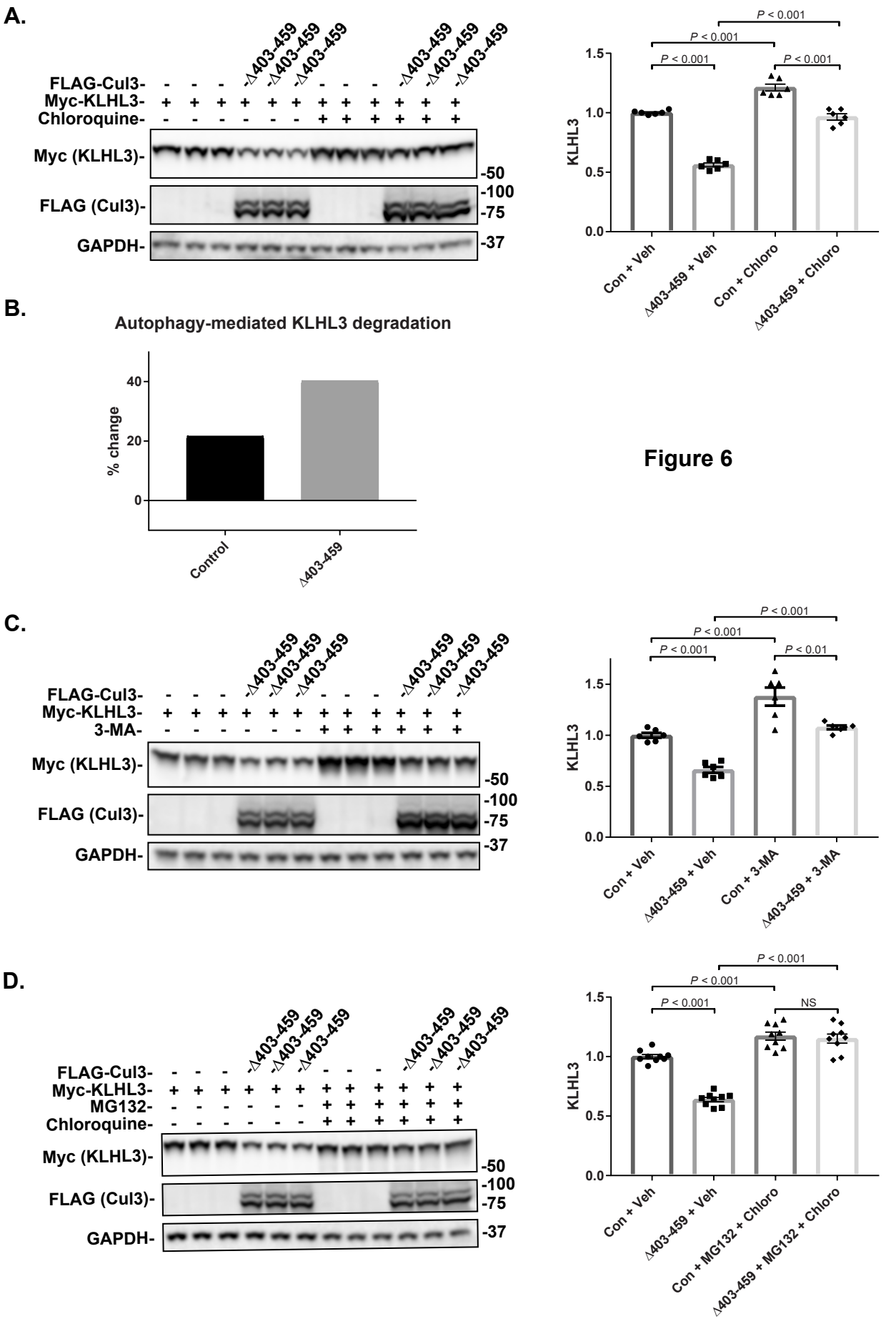
A.
FLAG-Cul3-
Myc-KLHL3-
Chloroquine-
-Δ403-459
Myc (KLHL3)-
FLAG (Cul3)-
GAPDH-
-50
-100
-75
-37
KLHL3
P < 0.001
Con + Veh
Δ403-459 + Veh
Con + Chloro
Δ403-459 + Chloro
B.
Autophagy-mediated KLHL3 degradation
% change
Control
Δ403-459
C.
3-MA-
P < 0.01
Con + 3-MA
Δ403-459 + 3-MA
D.
MG132-
NS
Con + MG132 + Chloro
Δ403-459 + MG132 + Chloro

Figure 6

Figure 7

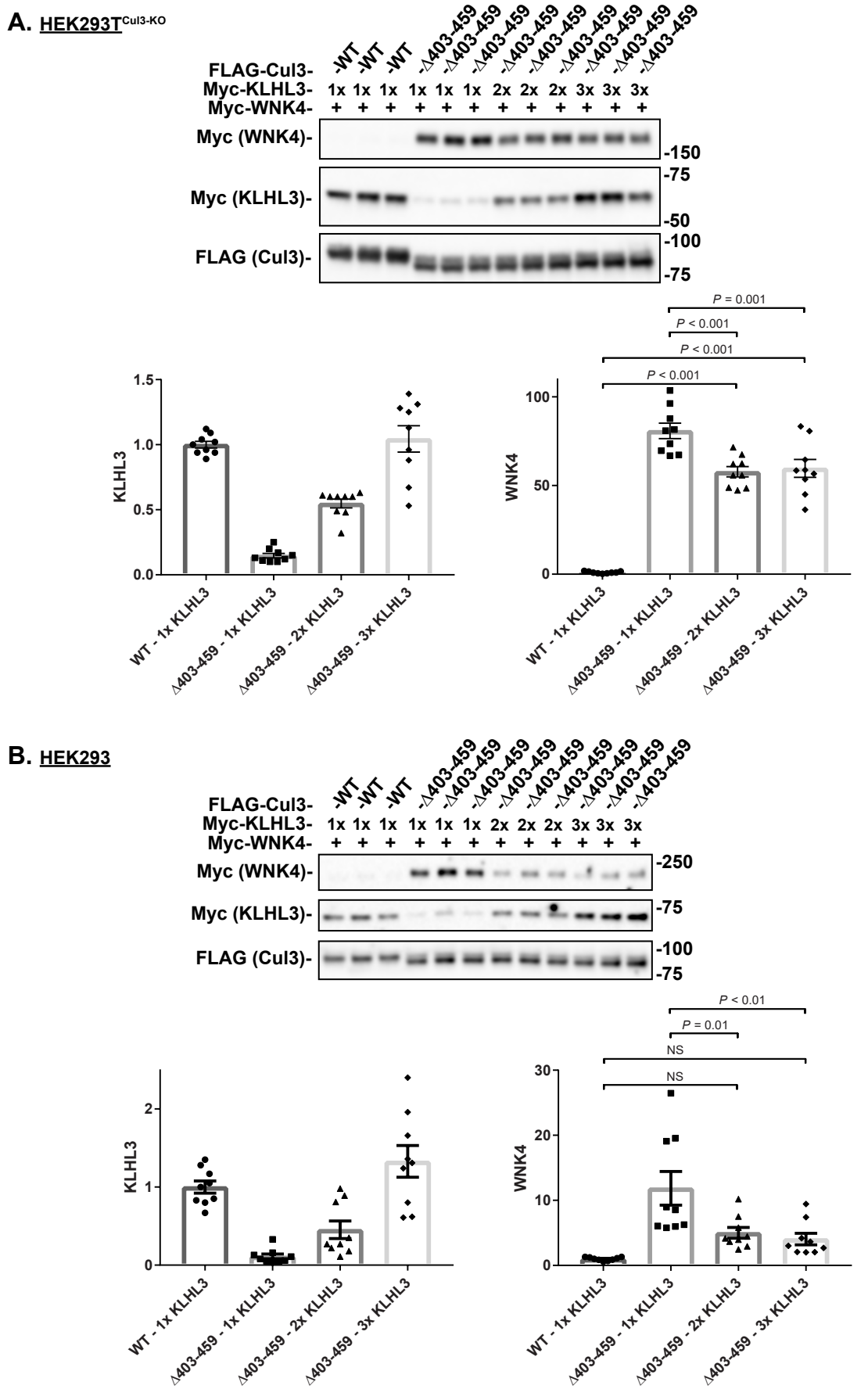
A. HEK293T Cul3-KO
FLAG-Cul3-
Myc-KLHL3-
Myc-WNK4-
-WT -WT -WT -Δ403-459 -Δ403-459 -Δ403-459 -Δ403-459 -Δ403-459 -Δ403-459 -Δ403-459 -Δ403-459 -Δ403-459
1x 1x 1x 1x 1x 1x 2x 2x 2x 3x 3x 3x
+ + + + + + + + + + + +
Myc (WNK4)-
Myc (KLHL3)-
FLAG (Cul3)-
-150
-75
-50
-100
-75
P = 0.001
P < 0.001
P < 0.001
P < 0.001
KLHL3
WNK4
WT - 1x KLHL3
Δ403-459 - 1x KLHL3
Δ403-459 - 2x KLHL3
Δ403-459 - 3x KLHL3
B. HEK293
-250
-75
-100
-75
P < 0.01
P = 0.01
NS
NS

Figure 8

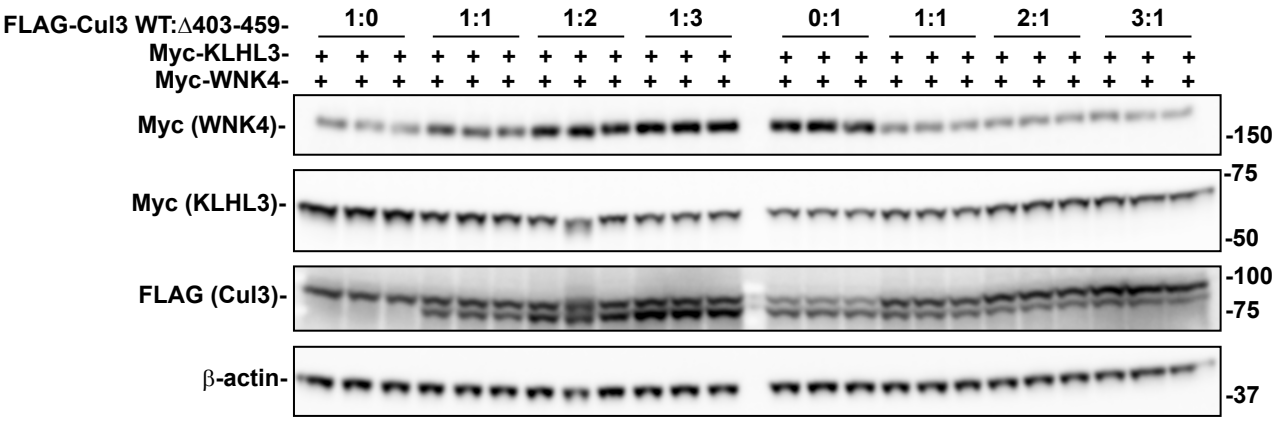
FLAG-Cul3 WT:Δ403-459-
1:0
1:1
1:2
1:3
0:1
1:1
2:1
3:1
Myc-KLHL3-
Myc-WNK4-
Myc (WNK4)-
Myc (KLHL3)-
FLAG (Cul3)-
β-actin-
-150
-75
-50
-100
-75
-37

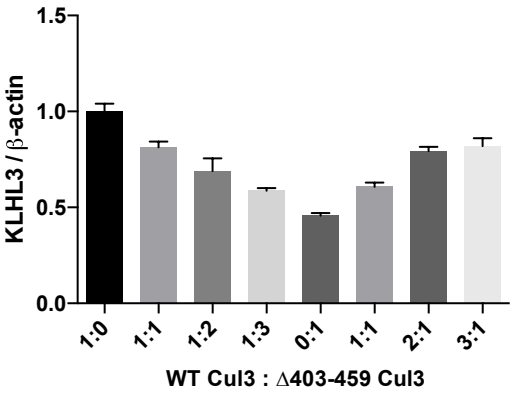
KLHL3 / β-actin
1.5
1.0
0.5
0.0
1:0
1:1
1:2
1:3
0:1
1:1
2:1
3:1
WT Cul3 : Δ403-459 Cul3

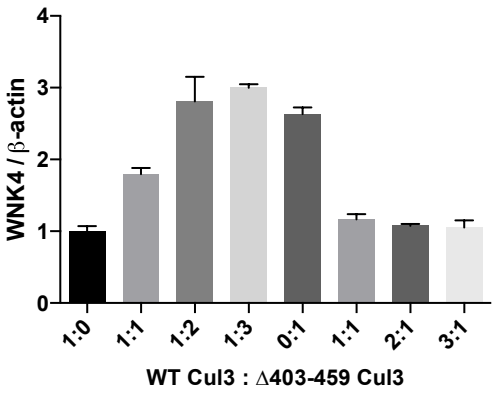
WNK4 / β-actin
4
3
2
1
0
1:0
1:1
1:2
1:3
0:1
1:1
2:1
3:1
WT Cul3 : Δ403-459 Cul3

Figure 9

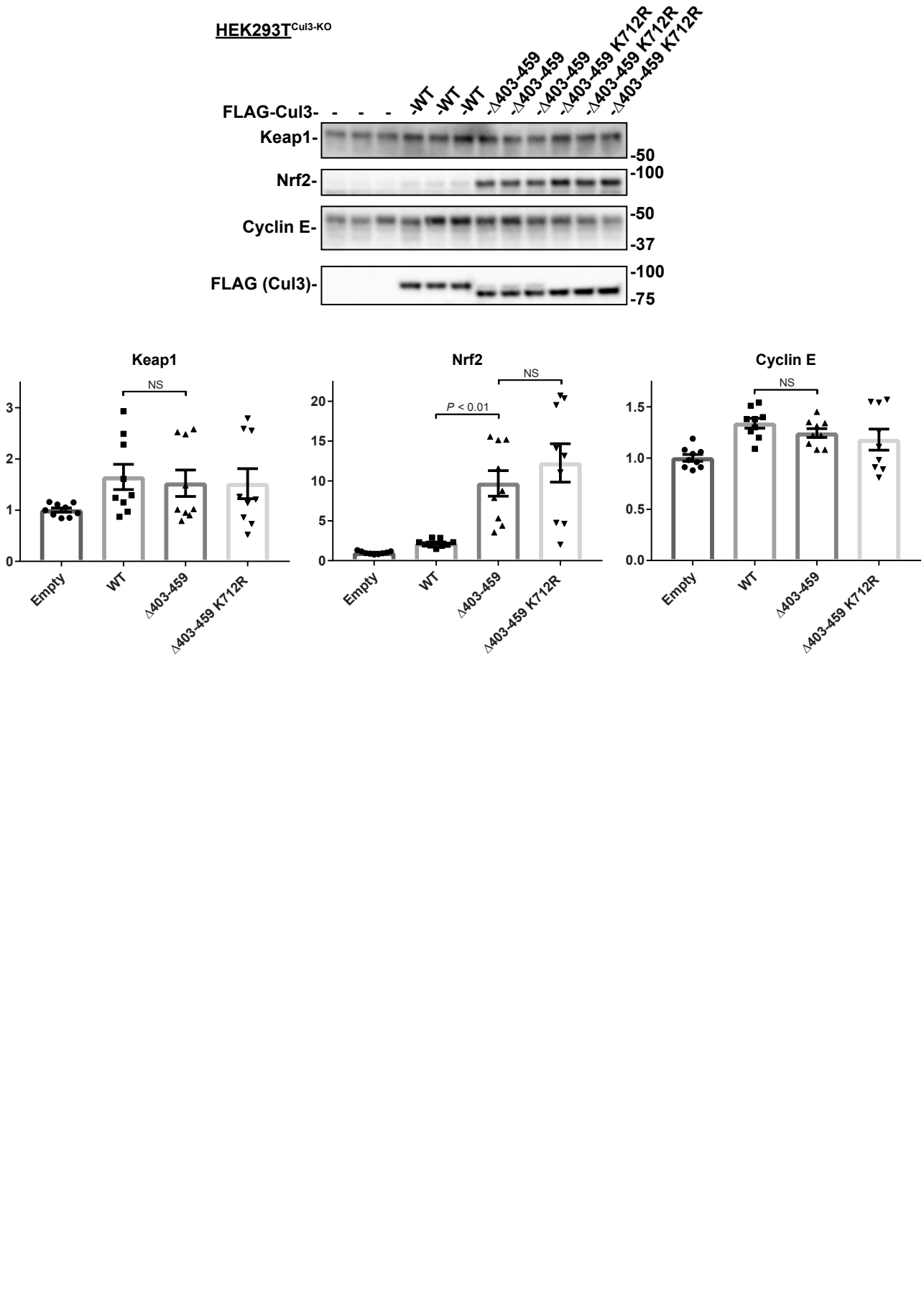
HEK293T Cul3-KO
FLAG-Cul3- - - - -WT -WT -WT -Δ403-459 -Δ403-459 -Δ403-459 -Δ403-459 K712R -Δ403-459 K712R -Δ403-459 K712R
Keap1-
Nrf2-
Cyclin E-
FLAG (Cul3)-
-50
-100
-50
-37
-100
-75
Keap1
NS
Empty
WT
Δ403-459
Δ403-459 K712R
Nrf2
NS
P < 0.01
Cyclin E
NS

Figure 10

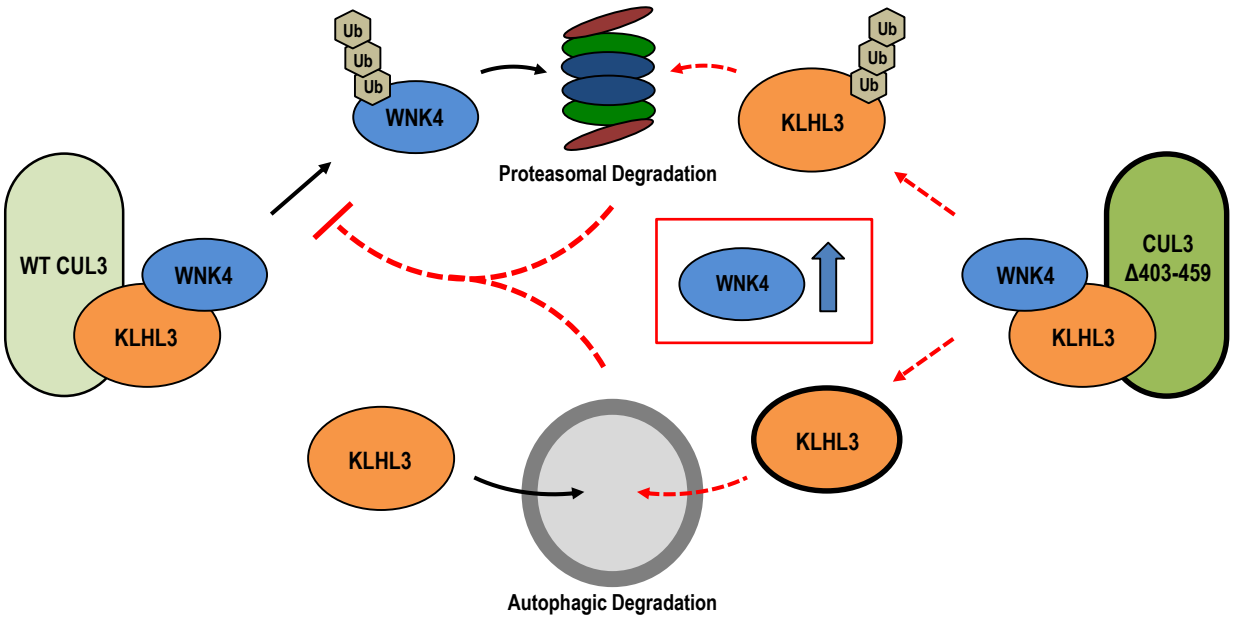
Ub
Ub
Ub
WNK4
Proteasomal Degradation
KLHL3
WT CUL3
WNK4
KLHL3
WNK4
CUL3
Δ403-459
WNK4
KLHL3
KLHL3
KLHL3
Autophagic Degradation